Microbial Cell Factories

RESEARCH

Open Access

Engineered biosynthesis and characterization of disaccharide-pimaricin

Xiaoshan Zuo[1†], Liqin Qiao[1†], Yao Dong[2], Xing Jin[3], Zhongyuan Ren[2*] and Hao Cui[1*]

Abstract

Background Disaccharide polyene macrolides exhibit superior water solubility and significantly reduced hemolytic toxicity compared to their monosaccharide counterparts, making them promising candidates for safer antifungal therapeutics. In this study, we engineered a *Streptomyces gilvosporeus* (pSET152-*nppY*) capable of producing disaccharide-pimaricin (DSP) through heterologous expression of the *nppY* gene, which encodes a glycosyltransferase responsible for the second sugar extension in the biosynthetic pathway.

Results The novel compound was structurally characterized and designated disaccharide-pimaricin (DSP), featuring an aglycone identical to pimaricin and a unique disaccharide moiety (mycosaminyl-α1–4-N-acetylglucosamine). A purification protocol for DSP was established. Compared to pimaricin, DSP demonstrated a 50% reduction in antifungal activity, a 12.6-fold decrease in hemolytic toxicity, and a remarkable 107.6-fold increase in water solubility. Growth analysis revealed a delayed growth cycle in the mutant strain, suggesting that *nppY* expression may impose additional metabolic burden. Optimization of the fermentation medium using a statistical design identified an optimal formulation, with a maximum DSP titer of 138.168 mg/L.

Conclusions This study underscores the potential of disaccharide polyene macrolides as safer antifungal agents and establishes a robust framework for engineering strains to produce these compounds. The findings provide critical insights into balancing biosynthetic efficiency and strain fitness, advancing the development of next-generation polyene antibiotics.

Keywords *Streptomyces gilposporeus*, Glycosyltransferase, Disaccharide-pimaricin, Water-soluble, Antifungal activity, Hemolysis

Background

Polyene macrolides are primarily utilized for treating fungal infections and preserving food due to their potent antifungal activities [1–3]. These compounds exert their antifungal effects by binding to ergosterol in fungal cell membranes, disrupting membrane integrity through three key mechanisms: vacuole fusion inhibition, impairment of membrane transport proteins, and ion leakage induction [4–8]. This unique mechanism of action minimizes the likelihood of fungal resistance development [9].

However, polyene macrolides exhibit a dual affinity for sterols in both fungal and mammalian cell membranes, particularly cholesterol in mammalian cells. This cross-reactivity can cause lysis of fragile mammalian cells

†Xiaoshan Zuo and Liqin Qiao have contributed equally to this work.

*Correspondence:
Zhongyuan Ren
rzy@jlict.edu.cn
Hao Cui
cuihao102@163.com
[1] School of Chemistry and Pharmaceutical Engineering, Jilin Institute of Chemical Technology, Jilin 132022, China
[2] College of Biology & Food Engineering, Jilin Institute of Chemical Technology, Jilin 132022, China
[3] Department of Anesthesiology, Affiliated Hospital of Beihua University, Jilin Institute of Chemical Technology, Jilin 132022, China

© The Author(s) 2025. **Open Access** This article is licensed under a Creative Commons Attribution-NonCommercial-NoDerivatives 4.0 International License, which permits any non-commercial use, sharing, distribution and reproduction in any medium or format, as long as you give appropriate credit to the original author(s) and the source, provide a link to the Creative Commons licence, and indicate if you modified the licensed material. You do not have permission under this licence to share adapted material derived from this article or parts of it. The images or other third party material in this article are included in the article's Creative Commons licence, unless indicated otherwise in a credit line to the material. If material is not included in the article's Creative Commons licence and your intended use is not permitted by statutory regulation or exceeds the permitted use, you will need to obtain permission directly from the copyright holder. To view a copy of this licence, visit http://creativecommons.org/licenses/by-nc-nd/4.0/.

(e.g., renal cells) and subsequent organ damage [10]. The molecular interactions within polyene antibiotics—specifically salt bridges and water bridges formed by post-modification groups—are critical for both structural stability and antifungal efficacy [4]. To address toxicity concerns, researchers have employed chemical or biological modifications of these post-modification groups to develop safer, more effective antifungal derivatives. Ideal compounds should exhibit enhanced ergosterol affinity, reduced cholesterol affinity, improved water solubility, and favorable pharmacokinetic properties. Key derivatives include decarboxylated, deglycosylated, dehydroxylated, and disaccharide-modified polyenes. Decarboxylated polyenes, for instance, often exhibit reduced hemolytic toxicity due to altered salt bridge interactions [10–15]. Davis et al. [9] demonstrated that substituting the carboxyl group in amphotericin B with a urea-based moiety yielded amphotericin B AU and MU, reducing hemolytic toxicity by half while doubling antifungal efficacy [9].

Glycosylation plays a pivotal role in polyene function: mycosamine removal abolishes both antifungal activity and hemolytic toxicity, as hydrogen bonding between mycosamine and ergosterol is critical for sterol binding [8, 16, 17]. Palacios et al. [18] further showed that the C2' hydroxyl group of mycosamine in amphotericin B forms a hydrogen bond with ergosterol's 3β hydroxyl group, confirming the structural basis for cholesterol binding specificity [18]. Terminal modifications, such as epoxy or hydroxyl groups introduced via cytochrome P450 enzymes, are critical for water bridge formation and maintain antifungal activity [11, 16, 19, 20]. While the mechanistic details of disaccharide modification remain understudied, Kim et al. [21] revealed that disaccharide addition precedes hydroxylation in nystatin analogs like Npp A1 [21]. Natural disaccharide-nystatins (e.g., Npp A1 and nystatin P1) exhibit 300-fold higher water solubility than nystatin, with tenfold lower hemolytic toxicity and half the antifungal potency [22, 23]. De Poire et al. [24] engineered *Streptomyces nodosus* to express the *nypY* gene, producing disaccharide-amphotericin B at 5% efficiency [24]. Subsequent studies by Walmsley et al. [25] improved this to 20–40% conversion by deleting the *amphL* gene (encoding hydroxylase), yielding disaccharide-8-deoxyamphotericins with MIC values comparable to amphotericin B (1.56 μmol/L) but reduced hemolytic toxicity [25]. De Poire et al. [24] and Walmsley et al. [25] suggests that disaccharide polyenes can be produced by integrating a second glycosyltransferase, and the resulting disaccharide polyenes have fewer side effects. Given the therapeutic potential of disaccharide-modified polyenes, this study aimed to engineer *Streptomyces gilvosporeus* by integrating the *nppY* gene to produce disaccharide-pimaricin (DSP). Pimaricin, a 26-membered tetraene macrolide, is clinically used for ocular fungal infections and food preservation. By characterizing DSP's structure and activity, we sought to advance the development of safer, more efficacious polyene-based antifungals.

Results

Construction of *S. gilvosporeus* (pSET152-nppY) via heterologous expression of *nppY*

Previous studies demonstrated that NppY catalyzes the addition of an (α1–4)–N–acetylglucosamine moiety as a second sugar group to nystatin during the biosynthesis of *Pseudonocardia autotrophica* [21, 22]. Based on this information, we explored heterologous expression of *nppY* in *S. gilvosporeus*, a native producer of pimaricin. The *nppY* gene was cloned into the pSET152 phiC31-based integrative vector under the control of the *hrdB* promoter and t_0 terminator, enabling chromosomal integration via site-specific recombination. The resultant recombinant strain, *S. gilvosporeus* (pSET152-*nppY*), was validated by PCR amplification of a 1,442-bp fragment spanning the *nppY* locus (Fig. S1).

Quantification of *nppY* gene transcription in *S. gilvosporeus* (pSET152-*nppY*)

To assess *nppY* transcriptional activity, reverse transcription PCR (RT-PCR) and quantitative RT-PCR (qRT-PCR) were performed using strain-specific primers. RT-PCR amplifications (30 cycles) revealed bands in both the mutant and wild-type strains, with significantly stronger signals in the recombinant strain (Fig. 1A). qRT-PCR (40

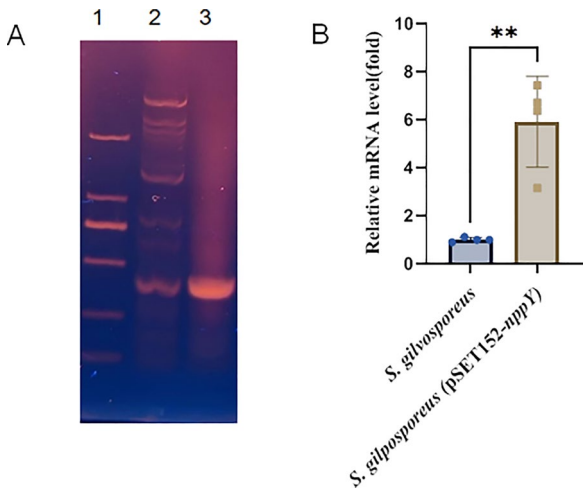

Fig. 1 Determination of *nppY* gene transcription levels in *S. gilvosporeus* (pSET152-*nppY*). **A** *S. gilvosporeus* and *S. gilposporeus* (pSET152-*nppY*) RT-PCR. **B** *S. gilvosporeus* and *S. gilposporeus* (pSET152-*nppY*) qRT-PCR

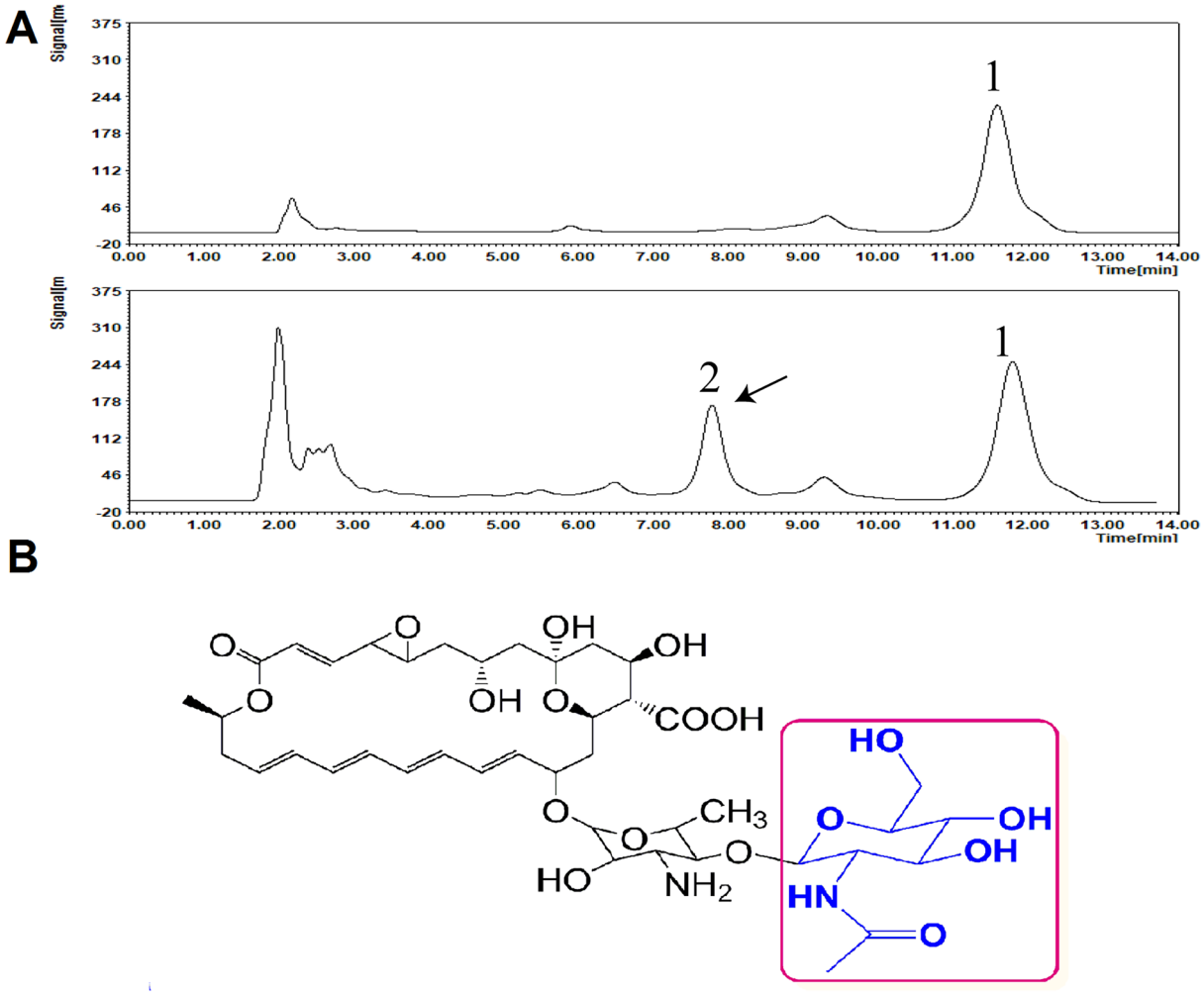

Fig. 2 HPLC analysis and spectral absorption of fermentation products. **A** HPLC analysis results show that the upper side corresponds to the fermentation product of *S. gilvosporeus*, and the lower side corresponds to the fermentation product of *S. gilvosporeus* (pSET152-*nppY*). The peak labeled 1 is pimaricin, and the peak labeled 2 is a new product. **B** The chemical structure of DSP produced by *S. gilvosporeus* (pSET152-*nppY*). The blue portion within the box represents the new glycosyl group attached via catalysis by NppY, specifically N-acetyl-glucosamine

cycles) confirmed a 5.91-fold upregulation of *nppY* transcription in *S. gilvosporeus* (pSET152-*nppY*) compared to the wild type (Fig. 1B), indicating robust expression of the heterologous gene.

Identification of novel products in *S. gilvosporeus* (pSET152-*nppY*)

To evaluate whether heterologous expression of *nppY* induces production of a pimaricin derivative in *S. gilvosporeus*, HPLC analysis was performed on fermentation supernatants from the mutant and wild-type strains. A standard curve was generated using pimaricin concentrations from 0 to 1000 µmol/L (Fig. S2). HPLC revealed a novel peak (peak 2) in the mutant strain's supernatant, with a shorter retention time (8 min) compared to pimaricin (peak 1, 12 min) (Fig. 2A). The spectral absorption profile of peak 2 matched that of pimaricin (Fig. S3A, B), confirming structural similarity. These results align with expectations for disaccharide-pimaricin (DSP).

To confirm the identity and characterize the new product, purification was performed via methanol extraction of both supernatant and sediment fractions. After rotary evaporation and vacuum drying, purified DSP and pimaricin crystals (95% purity) were obtained. Mass spectrometry (MS) analysis of the mutant strain's fermentation broth revealed m/z values of 666.4 ($[M+H]^+$) and 689.4 ($[M+Na]^+$) for pimaricin, alongside m/z 869.7 ($[M+H]^+$) for DSP and m/z 365.2 ($[M+H]^+$) for the N-acetylglucosamine moiety (Fig. S4A). The purified DSP exhibited distinct MS signals at m/z 869.8 ($[M+H]^+$) and 891.6 ($[M+Na]^+$),

consistent with the expected disaccharide structure (Fig. S4B). To further determine its chemical structure, the purified new product was identified by NMR, and the ^{1}H and ^{13}C chemical shifts were summarised (Table 1). The proton signal at δH, 8.55 in the 1H NMR spectrum (DMSOd6) is consistent with the N-acetyl group in NPP [22]. In contrast to the reported NMR data for pimaricin, a notable difference is the observation of the presence of acetyl groups, which is confirmed by the observation of a single heavy methyl proton signal at δH, 1.66, the corresponding carbon signal for methyl carbon at δC, 23.03, and the corresponding carbon signal for carbonyl carbon at 171.97. The formation of a disaccharide by linking N-acetylglucosamine to mycophenolate at the 4′ position was verified by a chemical shift from C-4′ to 78.24 ppm [14]. This information can be used to intuitively determine the addition of (α1–4)–*N*–acetyl–glucosamine to the new product. Therefore, the structure was shown in Fig. 2B, S. *gilvosporeus* (pSET152-*nppY*) can produce (α1–4)–*N*–acetyl–glucosamine–linked disaccharide–pimaricin.

Table 1 Chemical shift assignments of disaccharide–pimaricin (MeOD) recorded by 500 MHz NMR spectrometry

Position	Chemical shift (ppm)		Position	Chemical shift (ppm)	
	^{1}H NMR	^{12}C NMR[a]		^{1}H NMR	^{12}C NMR
1	–	167.05 s	22	6.17 m	137.4 d
2	6.09 d	125.5 d	23	5.63 m	129.67 d
3	6.5 m	146.24 d	24	2.31 m, 2.41 m	41.96 t
4	3.19 m	55.77 d	25	4.6 s	73.03 d
5	3.18 d,5	57.46 d	26	1.23 m	20.73 q
6	1.18 m,1.74 m	45 t	27	–	173.68 s
7	4.35 m	62.6 d	1′	4.53 d,10	99.82 d
8	1.41 m, 1.64 m	Over-lapped	2′	4.07 d	67.9 d
9	–	98.84 s	3′	2.87 d,10	59.59 d
10	1.26 m, 1.71 m	Over-lapped	4′	3.54 m	78.24 d
11	3.72 m	67.7 d	5′	3.46 m	69.53 d
12	0.93 m	Over-lapped	6′	1.03 d,20	18.04 q
13	4.31 m	71.6 d	1″	4.43 m	103.3 d
14	1.61 m, 2.27 m	40.99 t	2″	3.68 m	55.45 d
15	4.41 s	80.23 d	3″	3.56 m	75.32 d
16	6.02 m	137.01 d	4″	3.42 m	68.48 d
17	6.27 m	133.21 d	5″	3.44 m	72.02 d
18	6.45 m	134.62 d	6″	3.7 m, 4.02 m	61.97 t
19	6.19 m	130.26 d	$CO\underline{CH_3}$	1.66 m	23.03 q
20	6.22 m	133.59 d	$\underline{C}O$		171.97 s
21	6.24 m	133.12 d			

[a] The 8, 10 and 12 proton signals are highly overlapped and hard to be assigned

Comprehensive properties of pimaricin and DSP

In vitro antifungal assays against *Saccharomyces cerevisiae* revealed significant differences in potency between pimaricin and DSP. Pimaricin exhibited MIC_{50}, MIC_{90}, and MIC values of 0.82 ± 0.05, 1.14 ± 0.02, and 1.25 ± 0.01 μg/mL, respectively, while DSP displayed corresponding values of 1.79 ± 0.02, 2.47 ± 0.01, and 2.5 ± 0.03 μg/mL (Fig. S5A, Table 2). This indicates a ~ 50% reduction in antifungal efficacy for DSP compared to pimaricin (MIC ratio). DSP demonstrated markedly reduced cytotoxicity. The hemolytic concentration required to lyse 50% of erythrocytes (HC_{50}) was 165 ± 0.25 μg/mL for pimaricin and 2,083 ± 2.62 μg/mL for DSP (Fig. S5B, C). This represents a 12.6-fold decrease in hemolytic activity for DSP, underscoring its improved safety profile. By calculating the peak area of HPLC with the standard curve in Fig. S2, the solubility of pimaricin and DSP in water was 34.4 μg/mL and 3700 μg/mL, respectively, indicating that the water solubility of DSP was 107.6 times that of pimaricin.

Safe and effective antibiotics should have lower MIC values, higher HC_{50} values, and higher water solubility (S) values. The difference in the properties of the two antibiotics can be visualised in the radargram of Fig. 3, where the haemolytic toxicity and water solubility of DSP changed significantly compared to pimaricin. Moreover, the lower the T–value of the final result represented the better the application prospects of antibiotics. DSP exhibited a remarkable ~ 107.6-fold increase in aqueous solubility compared to pimaricin. Calculations based on HPLC peak area analysis (Fig. S2) yielded solubility values of 34.4 μg/mL for pimaricin and 3,700 μg/mL for DSP (Fig. S5D).

Optimization of fermentation medium

Single-factor experiments

Slow-release carbon sources were evaluated for their impact on DSP production. Corn flour and corn starch (2:1) (30 g/L) yielded the highest titer (24.4 mg/L) among tested slow-release substrates (Fig. 4A). For fast-release carbon sources, glucose (30 g/L) achieved the highest

Table 2 Comprehensive properties of pimaricin and disaccharide–pimaricin

	MIC_{50} (μg/mL)	MIC_{90} (μg/mL)	MIC (μg/mL)	HC_{50} (μg/mL)	S (μg/mL)
Pimaricin	0.82 ± 0.05	1.14 ± 0.02	1.25 ± 0.01	165 ± 0.25	34.4
DSP	1.79 ± 0.02	2.47 ± 0.01	2.5 ± 0.03	2083 ± 2.62	3700

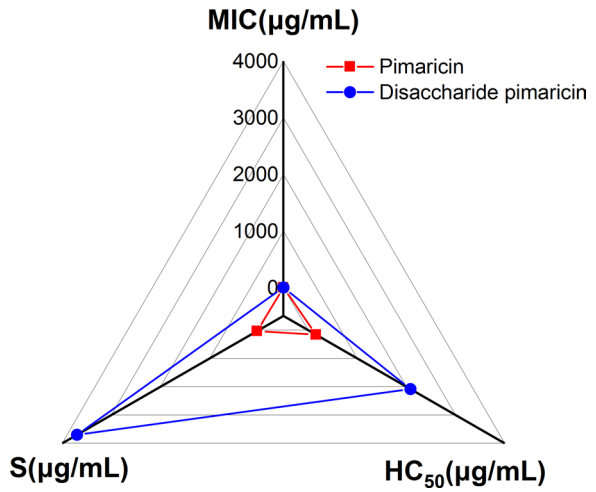

Fig. 3 Radargram of DSP and pimaricin about antimicrobial activity, hemolytic activity and solubility

titer (110.76 mg/L) (Fig. 4B). Among organic nitrogen sources, peptone (30 g/L) produced the highest titer (119.74 mg/L) and was selected for further optimization (Fig. 4C). Inorganic nitrogen sources were assessed, with $(NH_4)_2SO_4$ (30 g/L) yielding the highest titer (99.1 mg/L) (Fig. 4D). For phosphorus sources, K_2HPO_4 (30 g/L) produced the highest titer (75.23 mg/L) (Fig. 4E).

Plackett–Burman (PB) experimental design and results

Five critical factors identified in single-factor trials were subjected to PB design to evaluate their significance on DSP production. Each factor was tested at two levels: low (baseline concentration) and high (1.5×baseline). The response value was measured in terms of the DSP titer (mg/L) (Tables 3 and 4).

Statistical analysis (Minitab 18) revealed that glucose, $(NH_4)_2SO_4$, and K_2HPO_4 were the most significant

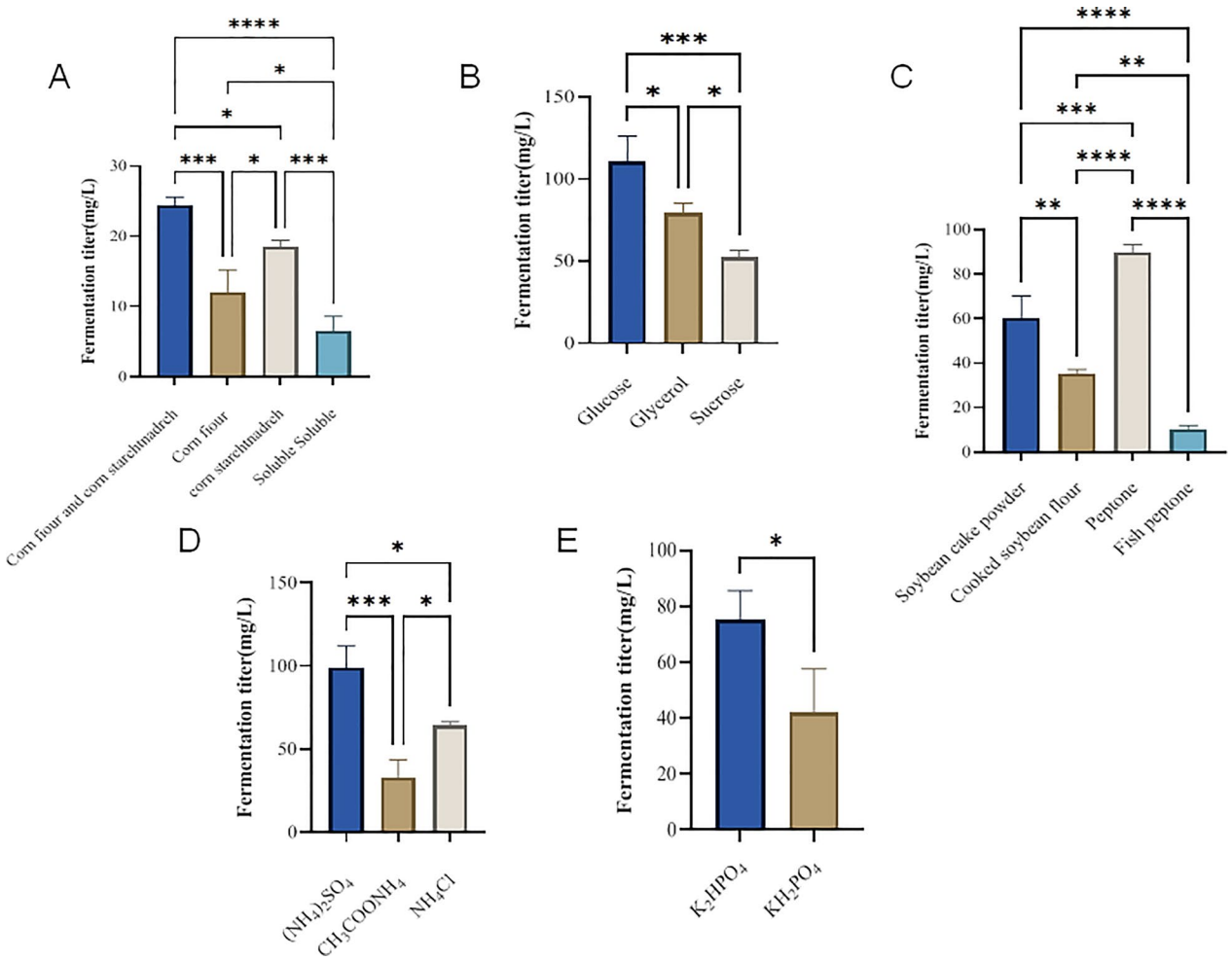

Fig. 4 The results of single-factor experiment. **A** The effect of delayed carbon sources on fermentation titer. **B** The effect of quick acting carbon sources on fermentation titer. **C** The effect of organic nitrogen sources on fermentation titer. **D** The effect of inorganic nitrogen sources on fermentation titer. **E** The influence of phosphorus source on fermentation titer

Table 3 Factors and levels of the Plackett–Burman experiment

Serial number	Considerations	Level	
		− 1	+ 1
X_1	Corn flour and corn starch	30 g/L	45 g/L
X_2	Glucose	30 g/L	45 g/L
X_3	Peptone	30 g/L	45 g/L
X_4	$(NH_4)_2SO_4$	2.5 g/L	3.75 g/L
X_5	K_2HPO_4	0.2 g/L	0.3 g/L

factors influencing DSP production. A first-order regression model was derived to predict DSP titers:

$$Y = 95.87 - 3.99X_1 + 16.62X_2 - 6.47X_3 + 13.17X_4 - 1.64X_5$$

where Y, X_1, X_2, X_3, X_4, and X_5 represent DSP titer, corn flour/corn starch, glucose, peptone, $(NH_4)_2SO_4$, and K_2HPO_4, respectively.

The Plackett–Burman (PB) analysis (Table 5) revealed that glucose and $(NH_4)_2SO_4$ exhibited significant positive effects on DSP production ($P < 0.05$), while K_2HPO_4 demonstrated a significant negative effect ($P < 0.05$). Despite its negative influence, K_2HPO_4 was retained as a critical factor due to its relatively lower P-value compared to other non-significant variables. This triad of factors (glucose, $(NH_4)_2SO_4$, and K_2HPO_4) was advanced to subsequent optimization steps.

Steepest ascent pathway to optimize factor levels

A steepest ascent experiment was conducted to identify the region of maximum DSP titer, guided by PB results. As shown in Table 6, glucose was increased by 2.5 mg/mL per step. $(NH_4)_2SO_4$ was increased by 0.125 mg/mL per step. K_2HPO_4 was decreased by 0.002 mg/mL per step. And the maximum DSP titer reached to 108.59 mg/L was in the group NO. 1 which in the concentration of glucose, $(NH_4)_2SO_4$, and K_2HPO_4 at 45 mg/mL, 2.5 mg/mL, and 0.2 mg/mL, respectively. These levels were selected for further refinement via response surface methodology (RSM).

Table 4 Plackett–Burman experimental design and results

Serial number	X_1	X_2	X_3	X_4	X_5	Titer (mg/L)
1	1	1	1	− 1	1	67.27
2	1	− 1	− 1	− 1	1	60.04
3	− 1	− 1	− 1	1	1	81.15
4	− 1	1	1	− 1	1	97.62
5	1	− 1	1	− 1	− 1	83.73
6	− 1	− 1	1	1	1	74.53
7	− 1	1	− 1	− 1	− 1	138.85
8	1	− 1	1	1	− 1	81.14
9	− 1	− 1	− 1	− 1	− 1	92.87
10	1	1	− 1	1	1	125.98
11	− 1	1	1	1	− 1	138.32
12	1	1	− 1	1	− 1	128.12

Table 5 Results of Plackett–Burman experimental analysis

Item	Effect	Ratio	Std Error	T-value	p-value	Variance inflation factor
		95.87	5.18	18.52	0.000	
Corn flour and corn starch	− 7.97	− 3.99	5.18	− 0.77	0.470	1.00
Glucose	33.25	16.62	5.18	3.21	0.018	1.00
Peptone	− 12.94	− 6.47	5.18	− 1.25	0.258	1.00
$(NH_4)_2SO_4$	26.35	13.17	5.18	2.54	0.044	1.00
K_2HPO_4	− 23.27	− 11.64	5.18	− 2.25	0.066	1.00

Table 6 Steepest ascent experimental design and results

Serial number	Mass concentration of impact factor (mg/mL)			Titer(mg/L)
	Glucose	$(NH_4)_2SO_4$	K_2HPO_4	
1	45	2.5	0.2	108.59
2	46.5	2.635	0.18	40.42
3	4.8	2.75	0.16	57.07
4	4.95	2.875	0.14	26.89
5	5.1	3.0	0.12	41.58
6	5.25	3.125	0.10	29.62

Box-Behnken experimental design and results

A three-factor, three-level Box-Behnken design was implemented using Design Expert 8.0.6. The factors and central points were glucose (A) in 45 mg/mL, $(NH_4)_2SO_4$ (B) in 2.5 mg/mL, and K_2HPO_4 in 0.2 mg/mL (C) with the step sizes of 2.5 mg/mL, 0.5 mg/mL, and 0.05 mg/mL, respectively. Quadratic regression equation for DSP titer (Table 7):

$$Y = 135.64 + 5.93A - 1.88B + 10.80C - 2.56AB - 8.84AC + 3.15BC - 32.97A^2 - 19.87B^2 - 20.11C^2$$

where Y, A, B, and C represent DSP titer, glucose, $(NH_4)_2SO_4$, and K_2HPO_4, respectively.

The quadratic regression model was rigorously validated using analysis of variance (ANOVA). The model exhibited significant predictive power ($P<0.05$), with an adjusted R^2 value of 93.68% (Table 8), indicating excellent agreement between predicted and experimental values. The lack-of-fit term ($P>0.05$) confirmed that the model adequately described the relationship between factors and the response (DSP titer). Residual analysis further validated model robustness: residuals were normally distributed and showed no discernible pattern when plotted against predicted values (Fig. 5), reinforcing the absence of systematic errors. Among the model items, the primary terms A and B were not significant, while C had a significant effect; the secondary terms A^2, B^2 as well as C^2 were significant, while the interaction terms AB, AC and BC were not significant. These findings suggest that the relationship between the factors and DSP yield is governed by quadratic effects rather than linear or interactive dependencies.

Figure 6 shows the contour plots and interaction analysis of glucose and $(NH_4)_2SO_4$. Elliptical contours indicate significant interaction between these factors. The 3D surface plot reveals a titer maximum at optimal concentrations of glucose and $(NH_4)_2SO_4$. Elliptical contours again suggest significant interaction of glucose and K_2HPO_4, with a titer peak at balanced concentrations (Fig. 7). In the group of $(NH_4)_2SO_4$ and K_2HPO_4 (Fig. 8), circular contours imply no significant interaction, yet the 3D plot shows a titer maximum at specific concentrations.

Table 7 Box-Behnken experimental design and results

Serial number	Mass concentration (mg/mL)			Titer(mg/L)
	Glucose	$(NH_4)_2SO_4$	K_2HPO_4	
1	45	2.5	0.2	150.563
2	45	2.5	0.2	142.683
3	45	2	0.15	92.113
4	42.5	2.5	0.25	96.067
5	45	2	0.25	110.763
6	45	2.5	0.2	120.457
7	42.5	2.5	0.15	60.1333
8	45	3	0.25	105.513
9	42.5	3	0.2	79.9967
10	45	2.5	0.2	129.463
11	42.5	2	0.2	70.8333
12	45	3	0.15	74.2567
13	45	2.5	0.2	135.053
14	47.5	3	0.2	89.647
15	47.5	2	0.2	90.743
16	47.5	2.5	0.15	86.7467
17	47.5	2.5	0.25	87.3267

After response optimization analysis, the optimal concentrations of the three main factors were determined: glucose at 45.144 mg/mL, $(NH_4)_2SO_4$ at 2.484 mg/mL, and K_2HPO_4 at 0.213 mg/mL. Under the established fermentation conditions, the maximum fermentation titer of DSP was predicted to be up to 137.212 mg/L. Fermentation of DSP obtained by response surface optimization The medium was formulated as follows: corn flour 20 mg/mL, corn starch 8 mg/mL, glucose 45 mg/mL, peptone 30 mg/mL, $(NH_4)_2SO_4$ 2.48 mg/mL, K_2HPO_4 0.21 mg/mL, NaCl 0.2 mg/mL, $MgSO_4$ 0.2 mg/mL, $FeSO_4$ 0.2 mg/mL, $CaCO_3$ 5 mg/mL.Under these conditions, the experimental fermentation achieved a DSP titer of 138.168 mg/L, closely matching the predicted value, thereby validating the robustness of the RSM-derived model.

Effect of heterologous expression of NppY on mycelial growth in *S. gilvosporeus*

The seed growth curve (Fig. 9A) shows that *S. gilvosporeus* (pSET152-*nppY*) grows slowly before 12 h, with 12–36 h being the logarithmic growth phase of the cell, 36–42 h being the stable growth phase of the cell, and entering the decay phase after 54 h. According to the curve, the seeds aged of 30–40 h have the best quality and are suitable for fermentation culture. Compared

Table 8 Analysis of Variance (ANOVA) of the Response Surface Quadratic Model

Source	Sum of squares	df	Mean square	F-value	p-value	
Model	10,417.98	9	1157.55	11.54	0.0020	Significant
a-glucose	281.24	1	281.24	2.80	0.1380	
B-NH_4SO_4	28.27	1	28.27	0.2818	0.6120	
C-K_2PO_4	933.55	1	933.55	9.13	0.0186	
AB	26.31	1	26.31	0.2623	0.6243	
AC	312.47	1	312.47	3.11	0.1210	
BC	39.73	1	39.73	0.3960	0.5491	
A^2	4575.79	1	4575.79	45.61	0.0003	
B^2	1662.87	1	1662.87	16.57	0.0047	
C^2	1702.70	1	1702.70	16.97	0.0045	
Residual	702.29	7	100.33			
Lack of fit	160.97	3	53.66	0.3965	0.7634	Not significant
Pure error	541.32	4	135.33			
Cor total	11,120.27	16				
R^2	0.9368					
Adjusted R^2	0.8556					
C.V.%	9.89					
Std.Dev	10.02					
Mean	101.32					
Predicted R^2	0.6923					
Adeq precision	10.2374					

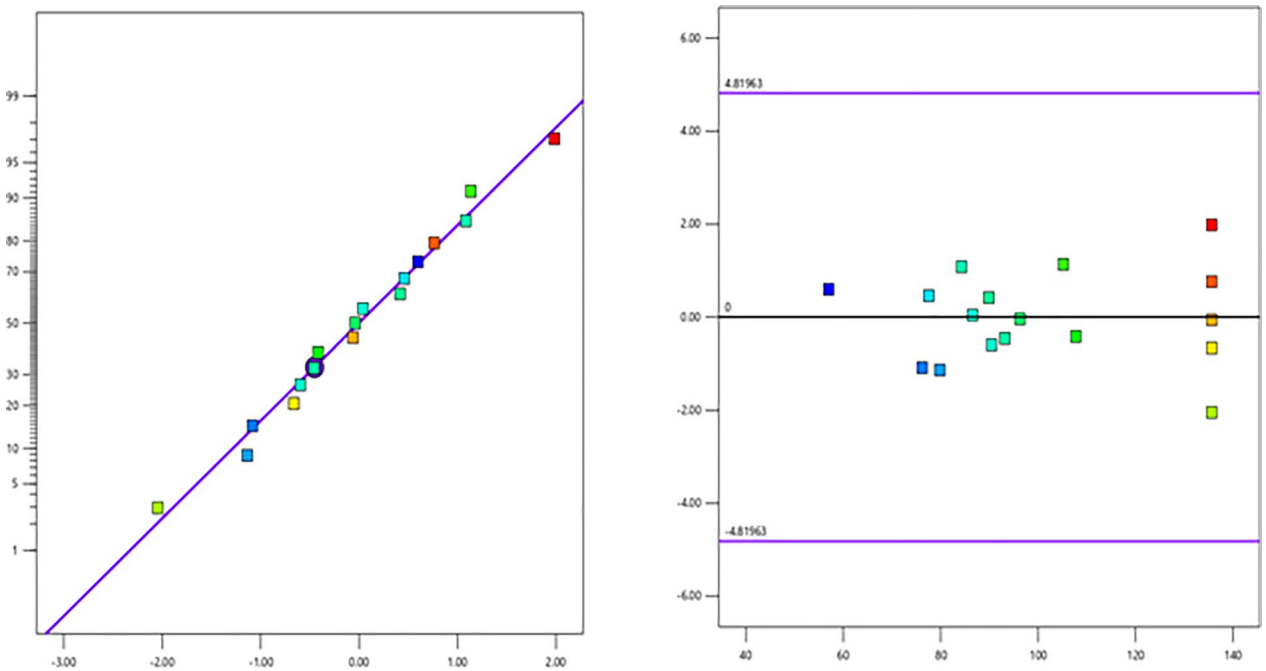

Fig. 5 Model residuals and predicted values

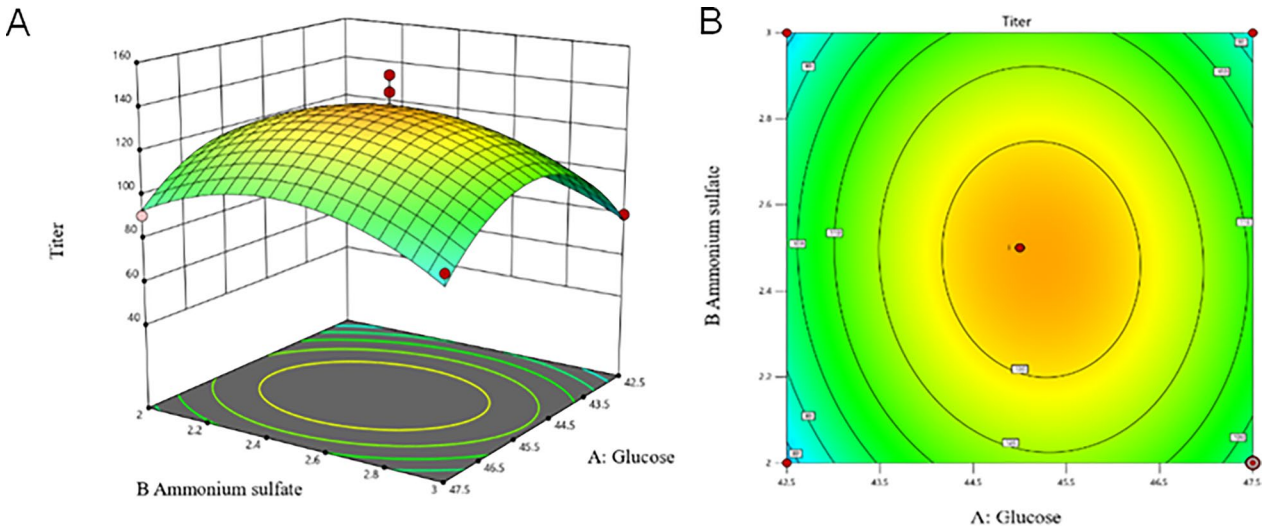

Fig. 6 Contour plots and response surfaces showing the effects of glucose and $(NH_4)_2SO_4$ on the fermentation titer of DSP

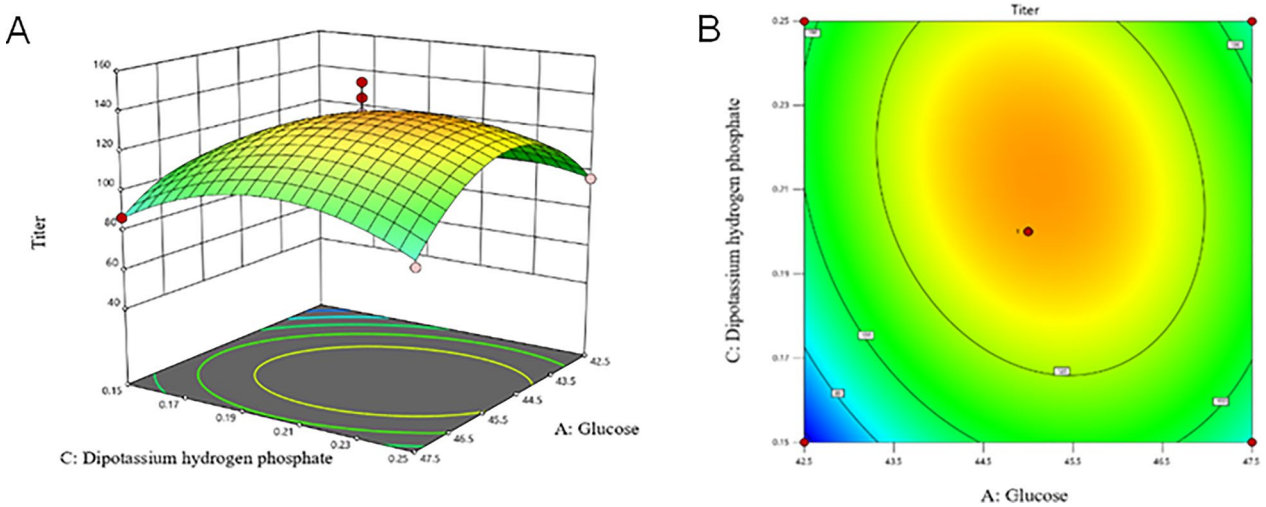

Fig. 7 Contour plots and response surfaces showing the effects of glucose and K_2HPO_4 on the fermentation titer of DSP

with the wild type, the shape of the seed growth curve did not change, but the growth cycle was delayed by 6 h. In addition, the growth curve shows that the growth of *S. gilvosporeus* (pSET152-*nppY*) was consistently lower than that of the original strain. Microscopic observations (optical microscopy at 100 × magnification and scanning electron microscopy (SEM, × 8000) at 25 h) revealed no significant differences in mycelium morphology between the two strains under light microscopy (Fig. S6). The results of ESM showed that the mycelium of the original strain had a smooth surface and thick mycelium, while the mycelium of the mutant strain was relatively elongated and had a less smooth surface (Fig. 9B, C).

Distribution and yield of DSP

To investigate the effect of temperature on DSP synthesis, *S. gilvosporeus* (pSET152-*nppY*) was cultured in the optimized fermentation medium at 26 ℃, 28 ℃, 30 ℃, and 32 ℃. Results showed no DSP production at 26 ℃ and 32 ℃, indicating that *S. gilvosporeus* (pSET152-*nppY*) is temperature-sensitive for secondary metabolic production of DSP. As shown in the bar chart (Fig. 10), between 96 and 120 h of fermentation, DSP production

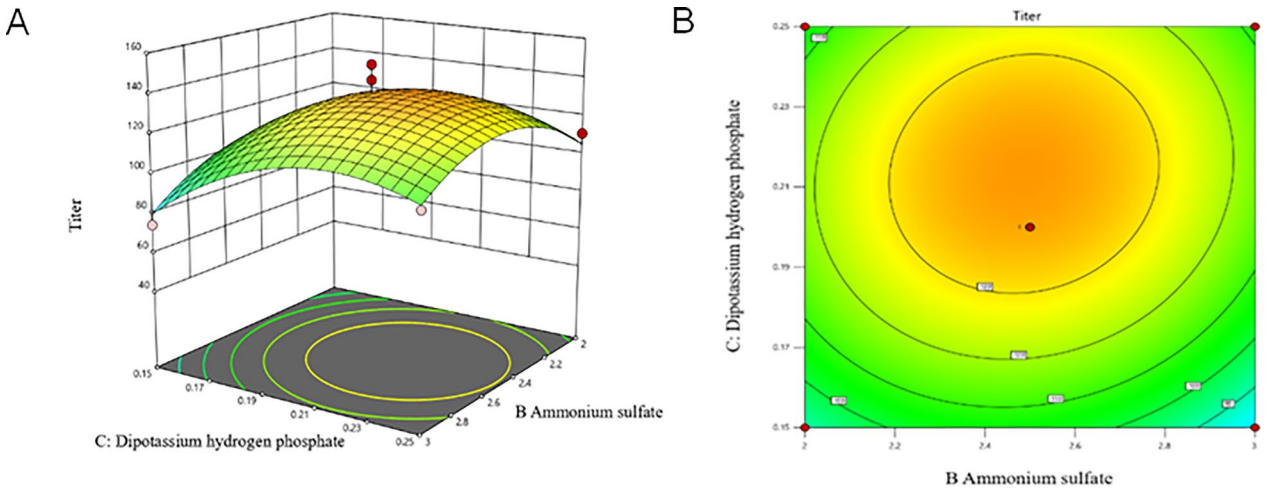

Fig. 8 Contour plots and response surfaces showing the effects of $(NH_4)_2SO_4$ and K_2HPO_4 on the fermentation titer of DSP

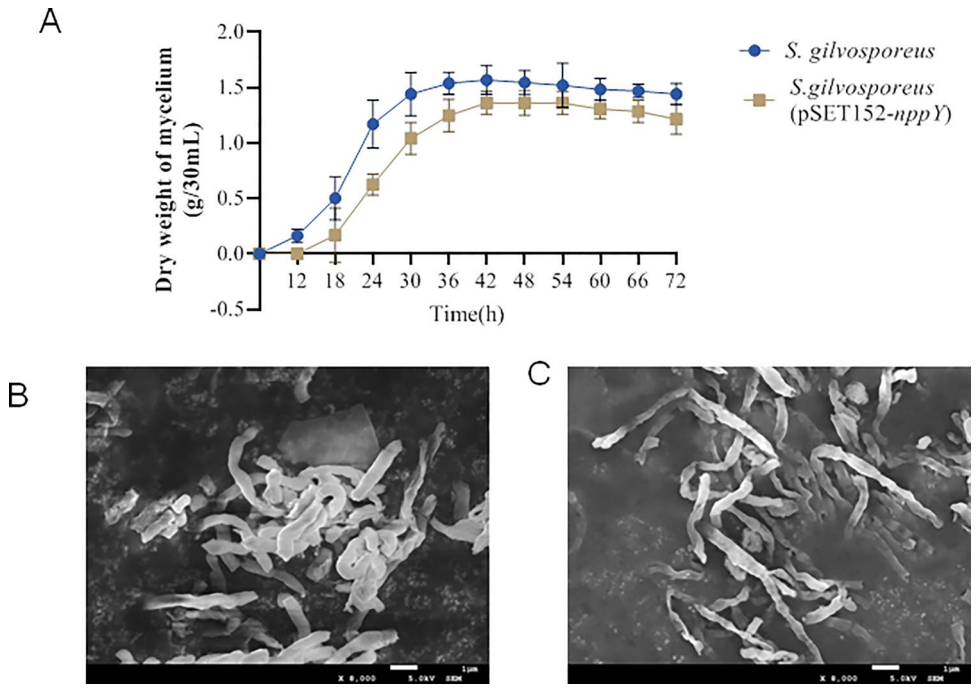

Fig. 9 Effect of heterologous expression of NppY on mycelial growth in *S. gilvosporeus* **A** Seed growth curves of *S. gilvosporeus* and *S. gilvosporeus* (pSET152-*nppY*) grown in seed culture medium for 0–72 h. The growth status of seeds every 6 h by weighing the wet weight of 30 mL of mycelium after centrifugation at 5000 × *g* for 10 min. **B** The scanning electron microscope images of the mycelia of *S. gilvosporeus* at 1 μm (×8000). **C** The scanning electron microscope images of the mycelia of *S. gilvosporeus* at 1 μm (×8000)

at 28 ℃ exceeded that at 30 ℃. Furthermore, DSP synthesis initially increased and then decreased between 96 and 120 h, peaking at 108 h. Thus, the optimal fermentation conditions for *S. gilvosporeus* (pSET152-*nppY*) were determined as 28 ℃ for 108 h. Additionally, HPLC analysis was performed on the supernatant of the fermentation medium and the mycelial extract of *S. gilvosporeus* (pSET152-*nppY*). The results revealed the distribution of DSP in both fractions under different conditions. Specifically, the supernatant contained 41% of total polyene macrolides as DSP, while mycelial extracts accounted for 33%. Overall, *S. gilvosporeus* (pSET152-*nppY*) achieved a 38% conversion efficiency

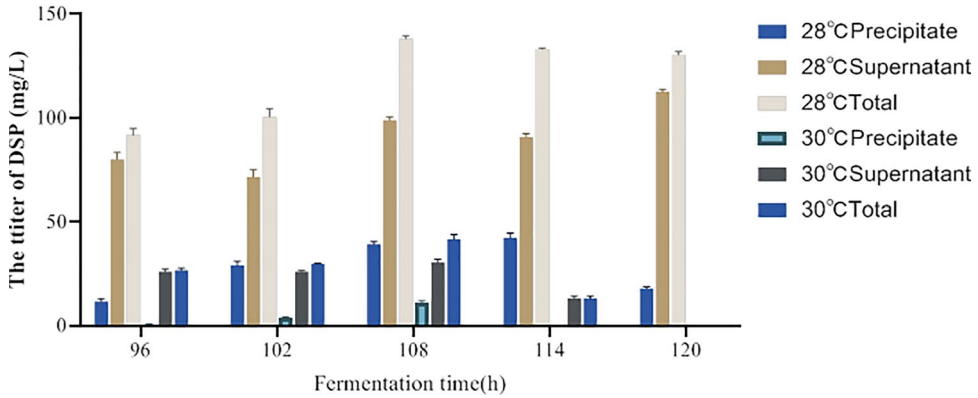

Fig. 10 The yield of DSP at different times and temperatures. The yield of DSP was investigated at two different temperatures, 28 °C and 30 °C, across five different time points: 96, 102, 108, 114, and 120 h. The study also examined the distribution of DSP in both the centrifuged pellet (cell sediment) and the supernatant of the fermentation broth

of pimaricin to DSP, representing the highest reported yield for disaccharide polyene macrolides to date.

Growth dynamics and production kinetics of *S. gilvosporeus* and *S. gilvosporeus* (pSET152-*nppY*)

During the 0–24 h fermentation period, the pH values of the fermentation broth for both *S. gilvosporeus* and *S. gilvosporeus* (pSET152-*nppY*) remained comparable and decreased as fermentation time increased. This initial pH decline was attributed to intense consumption of carbon and nitrogen sources by actively growing mycelia. After 24 h, the pH continued to rise, followed by a slight decrease between 84–120 h of *S. gilvosporeus*. The pH declined between 24–48 h, rose sharply after 48 h, remained stable from 48–96 h, surged again between 96 and 108 h, and then decreased after 108 h of *S. gilvosporeus* (pSET152-*nppY*) (Fig. 11A). Both strains exhibited declining amino nitrogen levels of both strains decreased until 24 h, followed by a sustained increase from 24 to 72 h, continued decrease from 72 to 96 h, and sudden increase followed by decrease at 108 h (Fig. 11B). Higher sugar consumption in the early phase (0–48 h) supported mycelial growth, while a more gradual decline in the mid-late phase (48–96 h) reflected antibiotic biosynthesis. For the *S. gilvosporeus*, total sugar content decreased slightly from 0 to 48 h, followed by a sharp decline until 96 h, and a minor increase occurred at 108 h before final reduction. Similar trends were observed, with a transient sugar increase at 108 h followed by depletion in *S. gilvosporeus* (pSET152-*nppY*) (Fig. 11C). At 36 h of fermentation, the cell growth reached the late logarithmic phase, and antibiotic synthesis increased rapidly (Fig. 11D). By 48 h, the synthesis of the disaccharide product had stabilized relatively, and it began to further increase after 96 h, eventually reaching the maximum titer of disaccharide product synthesis at 108 h (Fig. 11E). Overall, there is a close correlation between the indices throughout the fermentation process. The pH level is indicative not only of the growth and metabolic state of microscopic organisms, but also affects the degree of nutrient utilisation by microorganisms. Sugar dynamics reflect dual roles of carbon sources in growth (early phase) and antibiotic synthesis (late phase). *S. gilvosporeus* (pSET152-*nppY*) exhibited delayed pH fluctuations and prolonged sugar utilization compared to the wild type.

Discussion

Previous studies have demonstrated that polyene macrolides with a second glycosyl moiety exhibit reduced in vitro toxicity compared to those bearing only a single mycosamine residue. Additionally, heterologous expression of a second glycosyltransferase (e.g., *NypY*) has been employed to introduce a second glycosyl group into polyene macrolides [22, 25]. In this study, the *nppY* gene, encoding a second glycosyltransferase, was heterologously expressed in three polyene macrolide-producing strains, successfully generating *S. gilvosporeus* (pSET152-*nppY*), a strain capable of producing disaccharide polyene macrolide (DSP).

In terms of products, in addition to a reduction in antifungal activity, the 12.6 times decrease in haemolytic toxicity and 107.6 times increase in water solubility improve the safety of DSP. Its overall properties surpass those of pimaricin, aligning with other disaccharide polyene macrolides. Notably, NPP (nystatin-derived disaccharide) demonstrates a 300-fold increase in solubility over nystatin [22, 24]. This discrepancy may stem from pimaricin's inherently higher solubility relative to amphotericin and nystatin.

The successful construction of *S. gilvosporeus* (pSET152-*nppY*) demonstrates that the *nppY* gene can be expressed independently of its native promoter and terminator, contrasting with the *nypY* gene's heterologous expression in *S. nodosus* or *S. albidoflavus*, which requires native regulatory elements [24]. Notably, *S. nodosus* only increases disaccharide-amphotericin production after *AmphL* hydroxylase deletion, yet its conversion efficiency remains inferior to that of DSP in this study [24, 25]. It was initially speculated that the reason for the high conversion efficiency of the DSP was due to its different post–modification enzymes. Precursors of amphotericin, tetramycin, and nystatin undergo final modification by hydroxylases [10, 26, 27], while pimaricin's final step involves epoxylase [28]. In addition, the presence of hydroxylase is always positively correlated with the production of polyene macrolides, while the presence of epoxidase is not significantly related to the production of polyene macrolides [16, 20, 29]. Further, it is speculated that hydroxylase plays a role similar to DNA recognition and repair in the synthesis of polyene macrolides, which can prevent incorrect antibiotic precursor synthesis. The second glycosyltransferase can synthesize disaccharide complexes, but cannot synthesize disaccharide polyene macrolide precursors. The MS results of the fermentation products of *S. gilvosporeus* (pSET152-*nppY*) also seem to suggest the rationality of this speculation, as not only signals corresponding to the DSP were found, but also signals corresponding to the mycosamine–(α1–4)–*N*–acetyl–glucosamine complex.

Due to the enhanced water solubility of DSP, it is distributed in both the supernatant and precipitate of the fermentation medium. Therefore, it is essential not only to extract antibiotics from the mycelium but also to purify from the supernatant. A purification method for DSP was described in the results, which primarily leveraged the high methanol solubility of DSP and the precipitation tendency of certain impurities in methanol solutions. The absence of further solvent volatilization (specifically methanol and water) during concentration, coupled with the retention of antibiotics and impurity crystals, was attributed to the observation that residual impurities remained soluble in both solvents after methanol extraction of the fermentation product. Repeated volatilization and dissolution proved ineffective for DSP purification, as this process increased antibiotic degradation or loss. Concurrently, it was observed that even after filtration, the concentrated extraction solution precipitated at high concentrations during prolonged storage, with accelerated crystallization at low temperatures. HPLC analysis confirmed that these crystals were non-antibiotic impurities. Consequently, prior to HPLC purification, concentrated solutions were subjected to low-temperature overnight treatment. This approach ensured unobstructed chromatographic column flow while increasing the DSP concentration ratio in the liquid phase. While this method may lack scalability for industrial production due to high methanol consumption and low chromatographic efficiency, it remains suitable for laboratory-scale purification, offering simplicity, ease of operation, and a purification rate exceeding 95%.

Preliminary strain analysis shows that the seed growth cycle of *S. gilvosporeus* (pSET152-*nppY*) is longer, which may be due to the reflection of metabolic stress in the primary metabolism of the mycelium as a result of expression of the *nppY* gene. The optimal cultivation time and temperature of *S. gilvosporeus* (pSET152-*nppY*), as well as the purification steps of the DSP, were also derived from these data. This information is great significance for the laboratory production of DSP and lay a foundation for the industrial production of DSP.

The factors were first screened using a one-way analysis and Plackett–Burman design, followed by a steepest climb test to identify the optimal principal factors. Regression models were then applied to correlate these factors with response values, enabling derivation of optimal parameter values and the optimal fermentation formulation. When *S. gilvosporeus* (pSET152-*nppY*) was cultivated under the optimized conditions (temperature and medium composition), the strain reached the late logarithmic growth phase at 36 h, coinciding with rapid antibiotic synthesis initiation. By 48 h, disaccharide product synthesis lagged behind pimaricin accumulation, likely due to the timing of glycosylation. The disaccharide transferase-mediated modification occurs during later stages of pimaricin synthesis, necessitating prior accumulation of the precursor before glycosylation can proceed. Synthesis of the disaccharide product resumed rapid increase after 96 h and peaked at its maximum titer by 108 h.

Conclusion

This study constructed a strain *S. gilvosporeus* (pSET152-*nppY*) that can produce DSP, and investigated its growth conditions, DSP production, metabolic kinetic parameters, transformation efficiency, and determination of the transcript levels of the *nppY* gene. We determined the structure and comprehensive properties of DSP, demonstrated a significantly higher level of transcription of the *nppY* gene in *S. gilvosporeus* (pSET152-*nppY*), and summarised the purification protocol for this antibiotic and optimised its fermentation medium. Although there are shortcomings in industrial production, it is very suitable for laboratory purification. Last but not least, a

discussion was conducted on some cases of adding a second sugar group for polyene macrolide antibiotics, and some possible reasons that may affect the addition of a second sugar group were proposed, which will help further research.

Materials and methods

Bacterial strains and growth conditions

The strains and plasmids used in this study are listed in Table S1. *Escherichia coli* strains were grown in LB broth (or on LB agar) at 37 ℃. For sporulation, all the *Streptomyces* strains were grown on No.5 agar (2% soluble starch, 0.1% beef extract, 0.001% $FeSO_4{\cdot}7H_2O$, 0.05% K_2HPO_4, 0.05% $MgSO_4{\cdot}7H_2O$, 0.1% KNO_3, and 0.05% NaCl) (pH 7.2 ± 0.1) at 28 ℃ for 7–9 days. Conjugation between *E. coli* ET12567 (pUZ8002) [30] and *S. gilvosporeus* were performed on MS agar (2% soya bean powder and 2% mannitol, after sterilisation add 2 mL 0.5 mmol/L of $MgCl_2$ per 100 mL). *Streptomyces* fermentation requires two cultivation stages at 28 ℃. Firstly, mature spores were inoculated into the seed medium (2.0% glucose, 0.6% peptone, 0.6% yeast powder, and 1.0%NaCl) (pH 7.2 ± 0.1) and incubated at 28 ℃for 36 h to allow spore germination, growth, and the formation of seed mycelium. And then 10% of the seed suspension is inoculated into the fermentation medium (3.0% soya bean, 0.8% corn starch, 2.0% corn meal, 3.0% glucose, 0.02% NaCl, 0.02% $MgSO_4$, 0.02% K_2HPO_4, 0.02% $FeSO_4$, 0.5% $CaCO_3$ (light), and 0.25% $(NH_4)_2SO_4$) (pH 7.2 ± 0.1) for 108 h of fermentation. *Saccharomyces cerevisiae* ATCC9763 was cultivated in broth containing 2% peptone, 2% glucose, and 1% yeast extract. Healthy human red blood cells (hRBCs) were obtained from the Red Cross Center for Blood, Jilin, China, which is responsible for the legal administration of human erythrocytes for clinical and scientific usage in Jilin.

Construction of *nppY* gene expression mutant *S. gilposporeus* (pSET152-*nppY*)

The *nppY* (GenBank Accession Number: KP419743) was synthesized and insert into *Nco*I–*Hin*dIII digested pUC57 to construct of plasmid pUC57–*nppY* (Sangon Biotech, Shanghai). The heterologous expression of *nppY* was accomplished via site-specific integration using pSET152 [31]. The *nppY* sequence was then cloned into the *Nco*I and *Hin*dIII digestion sites of pHJ904 [32] to obtain the plasmid pHJ904–*nppY* (Fig. 1A). The *Bam*HI site of pSET152 was digested and dephosphorylated, followed by purification of the linearized vector. The *PhrdB*–*nppY*–t_0 fragment, excised via *Bgl*II digestion, was ligated into the prepared vector to generate the integrative plasmid pSET152–*nppY* (Fig. S1B).

The integrative plasmid was first introduced into *E. coli* ET12567 (pUZ8002) via a $CaCl_2$ method [33] and then into *S. gilvosporeus* by conjugation (however, heat shock step was performed at 45 ℃ due to decreased heat-resistance of *S. gilvosporeus* spores) [34]. After incubation at 28 ℃ for 20 h, each plate was overlaid with a mixture of 1 mL apramycin and nalidixic acid, the final concentration of both drugs being 50 μg/mL. After absorbing of the drug by the agar, the plates were cultured for 7–9 d to obtain apramycin–resistant exconjugants at 28 ℃. The apramycin–resistant exconjugants were amplified on No.5 agar and verify by polymerase chain reaction (PCR) with primers *nppY*–F/R (CGGAAGCCGTTTT/GCGGATCGCTGGAC).

Total RNA extraction, RT-PCR, and qRT-PCR analysis

The presence of particulate matter in the fermentation medium complicated mycelial harvesting for total RNA isolation. Therefore, *S. gilvosporeus* and its mutants were cultured on fermentation agar medium plates covered with cellophane sheets. After incubation at 28 ℃ for 48 h, mycelia were scraped from the cellophane and immediately flash-frozen in liquid nitrogen. Total RNA was extracted using RNAiso Plus (TaKaRa, Japan), followed by DNase I (RNase-free, TaKaRa) treatment to eliminate genomic DNA contamination.

Primers P-lysA-S and P-lysA-AS (GTGTCGGCCAGCACATC/CACTGGGT TGGCGGAATC) were designed to amplify a 577 bp fragment within the lysA gene (encoding diaminopimelate decarboxylase) as a control. All DNase I-treated RNA samples were confirmed to be free of genomic DNA via PCR using the aforementioned primers. cDNA synthesis was performed using the PrimeScript RT Reagent Kit (TaKaRa). For transcriptional analysis of *nppY* in mutants, gene-specific primers *nppY*–P1/P2 (TGTCCGCCCCGCCCTG/CGCCCCCACCATCCGT) were designed and validated by PCR with chromosomal DNA as the template. First-strand cDNA synthesis: Reaction mixture: 4 μL of 5×PrimeScript buffer, 1 μL of PrimeScript RT Enzyme Mix I, 500 ng of total RNA, and RNase-free H_2O to a final volume of 20 μL. Reaction conditions: 37 ℃ for 15 min, followed by enzyme inactivation at 85 ℃ for 5 s. RT-PCR amplification: Reaction mixture: 0.5 μM of each primer, 2 μL of cDNA, and H_2O to a final volume of 20 μL. Cycling conditions: 25 cycles of 94 ℃ for 45 s, 60 ℃ for 30 s, and 72 ℃ for 45 s. PCR products were analyzed by 0.7% (w/v) agarose gel electrophoresis stained with ethidium bromide and visualized under a UV transilluminator. Employ the Applied Biosystems 7500 system (Thermo Fisher Scientific, USA) with the Maxima™ SYBR Green/ROX qPCR Master Mix. The reaction system comprises the following: Reaction mixture: 10 μL of MightAmp, 2 μL

of cDNA, 0.4 μL of each primer (at a concentration of 10 μmol/L), 0.4 μL of ROX, and 6.8 μL of ddH_2O. Set an appropriate reaction program: Pre-denature at 98 ℃ for 2 min, then perform 40 cycles of denaturation. Each cycle consists of 15 s at 98 ℃, 30 s at 60 ℃, and 30 s at 72 ℃, followed by a final melting curve analysis. Use the housekeeping gene *lysA* as an internal control and calculate the relative transcription level of the target gene *nppY* using the ΔΔCt method.

HPLC analysis of fermentation products from wild–type and mutant strains

To measure the yield of polyenes and their distribution in the fermentation medium, the fermentation medium was centrifuged (3000×*g* for 20 min), the supernatant was retained, and the precipitate was extracted with the same volume of methanol. It was filtered through 0.22 μm filters and subjected to HPLC (DAD230+, Elite, China) analysis. The HPLC was operated at a flow rate of 1 mL/min with a Diamonsil C18(2) column (200×4.6 mm, particle size of 5 μm) and detected at 304 nm at 25 ℃. The mobile phase is 60% methanol containing 1% formic acid. The standard used for HPLC was the natamycin standard from Shanghai Macklin Biochemical Technology Co., Ltd. (Catalog No. P871756, 98%). The natamycin concentration gradient was set at 1000 μmol/L, 500 μmol/L, 250 μmol/L, 125 μmol/L, 62.5 μmol/L, 31.25 μmol/L, and 15.625 μmol/L.

Purification method of DSP and pimaricin

To collect all the polyenes in the fermentation medium, mix the precipitation extract and the supernatant mentioned above, centrifuge the mixture (5000×*g* for 15 min) and collect the supernatant (step 2 of Fig. S5). Evaporate the methanol from the supernatant by rotary evaporator (step 3 of Fig. S5). Store the remaining liquid at 4℃ overnight, centrifuge (5000×*g* for 15 min) and collect the supernatant (step 4 of Fig. S5). After dissolving these precipitates, HPLC analysis shows that these precipitates are some impurities. Elite C18 reverse–phase chromatography (250×25 mm, particle size 5 μm) was used for purification. The retention time of the new product fermented by *S. gilvosporeus* (pSET152-*nppY*) is 20 min, and the retention time of pimaricin is 40 min. The eluent is manually collected (step 5 of Fig. S5). After impurity removal, it was purified by semi–preparative HPLC (Elite C18 reverse–phase chromatography (250×25 mm, particle size 5 μm)). The mobile phase and detection wavelength used for HPLC separation were with the same as in 2.3 section, with a flow rate of 4.5 mL/min.

HPLC–MS and NMR analysis

HPLC–MS analyses were obtained on a Varian 500-MS Liquid chromatography-mass spectrometry (Varian, USA). The nuclear magnetic resonance (NMR) data of ^{1}H and ^{13}C NMR spectra were recorded on a Bruker AV–500 MHz spectrometer (Bruker Bioscience, Billerica, MA, U.S.A.), and MeOD was used as a solvent.

In vitro analysis of antifungal and hemolytic activities

The in *vitro* antifungal activity assay referred to the previously described method [22, 35]. The test organism used for the antibiotics in *vitro* antifungal activity tests was *Saccharomyces cerevisiae*, which was cultured in 180 μL of medium (nutrient composition can be found in media, with an inoculum of 1000 CFU per well) and 20 μL of diluted antibiotic samples (the final concentration is 0–10 μg/mL) at 28 ℃ without shaking in 96 well plate. The growth of *S. cerevisiae* was measured by absorbance at optical density of 660 nm (OD_{660}) after 14, 16, 18, and 20 h. Data were plotted against the antibiotic concentration, and the values of MIC_{50} and MIC_{90} (minimum inhibitory concentrations causing 50% and 90% inhibition of cell growth) values were estimated from the regression curves.

Determine the in *vitro* hemolytic activity of antibiotics by monitoring their ability to cause erythrocyte lysis in defibrinated human blood under buffered conditions [36]. Add 1–2 mL of EDTA at a concentration of 0.1–0.2 mol/L to 1 mL of blood before extracting erythrocyte for anticoagulation. Centrifuge the anticoagulant and discard the supernatant, then gently wash the precipitate several times with the same volume of phosphate buffered saline (PBS) buffer. After centrifugation (3000×*g* for 10 min), clear the supernatant to collect the precipitated erythrocyte for later use. Prepare antibiotic samples with concentrations of 10–2000 μg/mL using DSMO. Mix 0.1 mL of different concentrations of antibiotics with 0.9 mL of PBS buffer containing 2.5% (22.5 μL) erythrocyte and soak in water at 37 ℃ for 30 min (0.1 mL of DSMO as negative control), then centrifuge the sample and measure the OD_{545} value (positive control is PBS buffer with suspended 2.5% erythrocyte, which is haemolysis rate of 100%). Finally, use the following formula to calculate the haemolysis rate and plot a standard curve.

$$Hemolysis\ rate = \frac{sample\ OD_{545} - positive\ control OD_{545}}{positive\ control\ OD_{545} - negative\ control\ OD_{545}} \times 100\%.$$

The values of HC_{50} (hemolytic concentrations causing 50% hemolysis) value were estimated from the regression curves. All the.

Solubility measurement

Dissolve 1 mg of DSP and 1 mg of pimaricin in 50 μL and 500 μL of 10 mmol/L of Tris–HCl solution (pH 7.0), respectively, and shake thoroughly for 15 min using a vortex oscillator. After centrifugation, the saturated aqueous solutions of DSP and pimaricin were diluted 50 and 5 times, respectively. The absorption peak at 304 nm was detect by HPLC to calculate the concentrations of the two water–saturated solutions which were the solubility of the antibiotics and were represented by solubility (S).

Comprehensive evaluation formula

In order to identify whether DSP has better application prospects based on the existing data, the calculation formula of the treatment index of Won et al. [37] was modified as follows [37]:

$$T = \frac{MIC}{HC_{50}} + \frac{MIC}{S}$$

Where T, MIC, HC_{50} and S represented comprehensive score of antibiotics, minimal inhibitory concentrations, hemolytic concentrations causing 50% hemolysis, and solubility of antibiotics, respectively.

Evaluation of strain growth conditions

The production of the DSP by cultivation of *S. gilvosporeus* (pSET152-*nppY*) mainly involves two stages: seed culture and fermentation culture. *S. gilvosporeus*

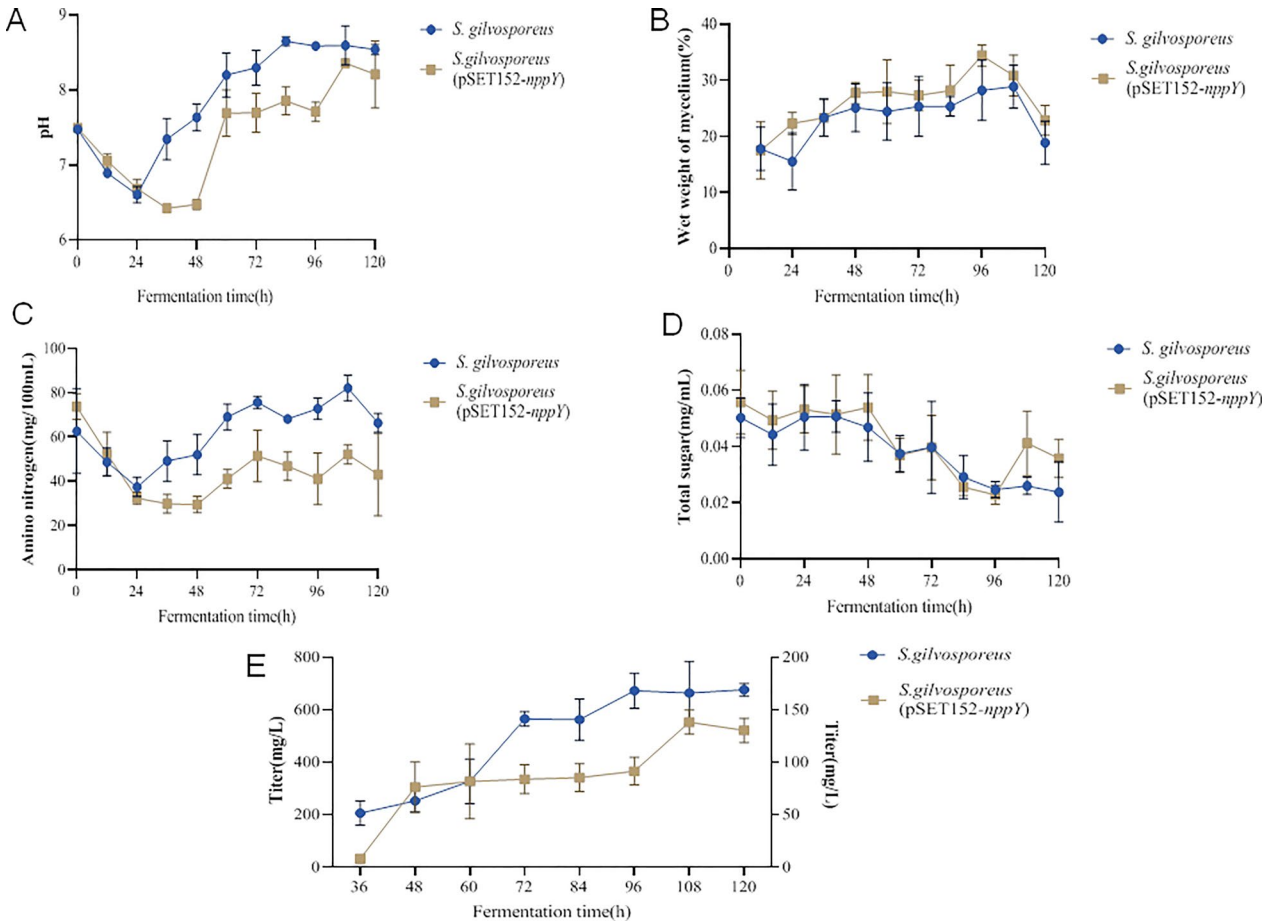

Fig. 11 Growth dynamics and production kinetics of *S. gilvosporeus* and *S. gilvosporeus* (pSET152-*nppY*). **A** pH. **B** Amino nitrogen. **C** Total sugar. **D** Mycelial wet weight. **E** Production of antibiotics

(pSET152-*nppY*) seeds are incubated for 72 h, and measure the growth status of seeds every 6 h by weighing the wet weight of 30 mL of mycelium after centrifugation at 5000×*g* for 10 min. Use the wild–type as a control and plot a seed growth curve. The culture temperatures of the pimaricin–producing strains mentioned in the literature include 26 ℃, 28 ℃, 30 ℃ and 32 ℃, and a series of 96–120 h cultivation was performed under each temperature condition. HPLC was used to analysis the concentration of polyene produced at each temperature and time period to determine the culture temperature and fermentation end-point.

Medium optimization

Single-factor experimental design

The fermentation medium of *S. gilvosporeus* served as the preliminary medium, primarily composed of corn flour (20 g/L), corn starch (10 g/L), glucose (30 g/L), soybean cake powder (30 g/L), and $(NH_4)_2SO_4$ (2 g/L)0.5 g/L, K_2HPO_4 0.2 g/L, NaCl 0.2 g/L, $MgSO_4$ 0.2 g/L, $FeSO_4$ 0.2 g/L, $CaCO_3$ 5 g/L, and pH was adjusted to 7.0–7.2. The single-factor method was employed to screen late-acting carbon sources, fast-acting carbon sources, organic nitrogen sources, inorganic nitrogen sources, and phosphorus sources. The optimal factor was identified based on fermentation titer under conditions where other variables were held constant.

Plackett–Burman design

Ased on the screening results of the single-factor test, an experimental design was conducted using Minitab software. Six medium components—corn flour, corn starch, glucose, peptone, $(NH_4)_2SO_4$ and K_2HPO_4 were selected, with twelve parallel experiments performed. In the design, "-1" denoted the low level and "1" the high level, and experiments were structured with fermentation titer as the response value.

Path of steepest ascent method

According to the regression model derived from the Plackett–Burman test, the primary factors influencing efficacy of glucose, $(NH_4)_2SO_4$ and K_2HPO_4 were identified. The step size for each factor's adjustment was determined based on the magnitude of effect values and their positive/negative direction, enabling rapid approximation of the maximum response region to establish the center point for subsequent response surface optimization.

Box-Behnken design

Based on the results of the Plackett–Burman (PB) and steepest climb experiments, a three-factor, three-level Box-Behnken design was constructed using Design Expert 8.0.6 software, comprising 17 experimental runs with five replications at the centroid. DSP fermentation titer was used as the response value.

To identify medium factor combinations maximizing DSP titer, a multivariate quadratic model was established using DSP titer as the response variable, formulated as:

$$Y = \beta_0 + \sum_{\mathrm{i}=1}^{\mathrm{n}} \beta_i X_i + \sum_{\mathrm{i}=1}^{\mathrm{n}} \beta_{ii} X_i^2 + \sum_{i<j}^{n} \beta_{ij} X_i X_j + \varepsilon$$

In this model, Y represents the predicted DSP titer; β_0 acts as the coefficient of the constant term, which acts as the underlying fixed value; β_i is the coefficient of the primary term of the independent variable X_i, reflecting its linear effect on titer; β_{ii} is the coefficient of the quadratic term of the independent variable X_i used to characterise the non-linear variation relationship; β_{ij} embodies the coefficient of the interaction effect between the independent variable X_i and other variables to show the synergistic influence of the variables; and ε denotes the unavoidable random error in the experimental process.

Analysis of metabolic process in mutant

The pH of the fermentation broth was measured using a pHS-3C pH meter. To measure the dry weight of mycelium, 1 mL of the seed culture solution was sampled every 6 h. The sample was centrifuged at 3000 rpm for 10 min, after which the supernatant was discarded. The remaining precipitate was placed in an oven at 60 ℃ and dried to a constant weight. Subsequently, it was taken out and weighed. For the amino nitrogen content test, a 5 mL pipette was used to accurately aspirate 2.5 mL of centrifugal supernatant into a 250 mL conical flask, followed by the addition of 50 mL of distilled water measured with a graduated cylinder. Two drops of $C_{15}H_{15}N_3O_2$ were added, then 0.1 mol/L HCl was pipetted into the conical flask until the solution turned light red. Subsequently, 0.05 mol/L NaOH solution was added until the solution turned orange. Next, a graduated cylinder was used to measure 4 mL of 18% CH_2O and added to the conical flask; the mixture was shaken thoroughly and left for 10 min. Eight drops of $C_{20}H_{14}O_4$, were then added, and 0.05 mol/L NaOH solution was introduced via an alkaline burette for titration until the mixture turned slightly red. The volume of NaOH consumed was recorded, and the amino nitrogen content was calculated using the formula.

For the determination of total sugar content, $C_6H_{12}O_6$ was used as the standard, and the sugar content was determined via the phenol–sulfuric acid method. Precisely 0.0503 g of anhydrous $C_6H_{12}O_6$ (dry and constant weight) was weighed and placed in a 50 mL volumetric

flask. Distilled water was added to dissolve and dilute the solution to the mark, yielding a glucose standard solution with an initial concentration of 1.00 mg/mL. Separately, 1.25 g of C_6H_6O was weighed and dissolved in distilled water to prepare a 5% C_6H_6O solution in a 25 mL volumetric flask. Serial dilutions of the glucose standard solution (0.2 mL, 0.4 mL, 0.6 mL, 0.8 mL, and 1.0 mL) were pipetted into 10 mL volumetric flasks and diluted to volume with distilled water. For sample analysis, 1 µL of fermentation broth was diluted with 999 µL of distilled water, mixed with 1 mL of C_6H_6O and 5 mL of H_2SO_4 solution, then incubated for 30 min. Absorbance was measured at 490 nm using a UV spectrophotometer (TU-1810), and the total sugar concentration was calculated by referencing the standard curve.

The seed mycelium of *S. gilvosporeus* and *S. gilvosporeus* (pSET152-nppY) was incubated for 25 h for morphological observation. Fresh mycelium was collected via centrifugation at 5000 rpm for 3 min. The samples were rinsed twice with PBS (pH 7.0) and fixed overnight at 4 ℃. Subsequently, the mycelium was rinsed three times with 500 µL PBS, followed by the addition of 1 mL of 2.5% glutaraldehyde solution. After three PBS rinses (500 µL each), 500 µL of 1% osmic acid was added, mixed thoroughly, and fixed for 1 h. The samples were rinsed three times with 500 µL PBS and subjected to graded ethanol dehydration (20%, 50%, 80%, and 100%) for 10 min each, followed by centrifugation at 5000 rpm for 3 min. The samples were then treated with 100% tert-butanol twice, centrifuged to remove supernatant, and incubated with 200 µL of pure acetone at 4 ℃ for 20 min. After centrifugation at 5000 rpm for 3 min, fresh acetone was added. Finally, the samples underwent critical point drying, coating, and morphological observation via scanning electron microscopy (Japan Electronics, JSM-7610F Plus).

Statistical analysis

Three parallel experiments were performed for all determinations. Experimental data were statistically processed by analysis of variance (ANOVA) combined with Duncan's multiple range test using SPSS 19.0 statistical software (SPSS Inc., Chicago, IL, USA) and results are presented as "mean ± standard error". A significant effect was considered when $P < 0.05$.

Supplementary Information

The online version contains supplementary material available at https://doi.org/10.1186/s12934-025-02742-9.

Supplementary material 1.

Acknowledgements
The authors gratefully acknowledge the Analytical and Testing Center of Jilin Institute of Chemical Technology for their assistance with electron microscopy analysis of the mycelium.

Author contributions
Xiaoshan Zuo: Methodology, Validation, Formal analysis, Investigation, Writing—review & editing. Liqin Qiao: Software, Validation, Investigation, Writing—original draft, Visualization, Project administration. Yao Dong: Data curation, Supervision, Project administration. Xing Jin: Visualization. Zhongyuan Ren: Writing—review & editing, Project administration. Hao Cui: Resources, Conceptualization, Data curation, Writing—original draft, Funding acquisition.

Funding
This work was supported by the Department of Science and Technology of Jilin province (grant number YDZJ202201ZYTS440), the National Natural Science Foundation of China (grant number 81903528), the Program of Jilin Provincial Development and Reform Commission (grant number 2022C043), and the Department of Education of Jilin Province (grant number JJKH20240320KJ).

Data availability
No datasets were generated or analysed during the current study.

Declarations

Ethics approval and consent to participate
Not applicable.

Consent for publication
This paper consists of original, unpublished work which is not under consideration for publication elsewhere.

Competing interests
The authors declare no competing interests.

Received: 13 September 2024 Accepted: 6 May 2025
Published online: 22 May 2025

References

1. Lemke A, Kiderlen AF, Kayser O. Amphotericin B. Appl Microbiol Biotechnol. 2005;68(2):151–62.
2. Mora-Duarte J, Betts R, Rotstein C, Colombo AL, Thompson-Moya L, Smietana J, et al. Comparison of caspofungin and amphotericin B for invasive candidiasis. N Engl J Med. 2002;347(25):2020–9.
3. Aparicio JF, Colina AJ, Ceballos E, Martín JF. The biosynthetic gene cluster for the 26-membered ring polyene macrolide pimaricin. A new polyketide synthase organization encoded by two subclusters separated by functionalization genes. J Biol Chem. 1999;274(15):10133–9.
4. Palacios DS, Dailey I, Siebert DM, Wilcock BC, Burke MD. Synthesis-enabled functional group deletions reveal key underpinnings of amphotericin B ion channel and antifungal activities. Proc Natl Acad Sci U S A. 2011;108(17):6733–8.
5. te Welscher YM, Jones L, van Leeuwen MR, Dijksterhuis J, de Kruijff B, Eitzen G, et al. Natamycin inhibits vacuole fusion at the priming phase via a specific interaction with ergosterol. Antimicrob Agents Chemother. 2010;54(6):2618–25.
6. te Welscher YM, van Leeuwen MR, de Kruijff B, Dijksterhuis J, Breukink E. Polyene antibiotic that inhibits membrane transport proteins. Proc Natl Acad Sci U S A. 2012;109(28):11156–9.
7. Gray KC, Palacios DS, Dailey I, Endo MM, Uno BE, Wilcock BC, et al. Amphotericin primarily kills yeast by simply binding ergosterol. Proc Natl Acad Sci U S A. 2012;109(7):2234–9.
8. Anderson TM, Clay MC, Cioffi AG, Diaz KA, Hisao GS, Tuttle MD, et al. Amphotericin forms an extramembranous and fungicidal sterol sponge. Nat Chem Biol. 2014;10(5):400–6.

9. Davis SA, Vincent BM, Endo MM, Whitesell L, Marchillo K, Andes DR, et al. Nontoxic antimicrobials that evade drug resistance. Nat Chem Biol. 2015;11(7):481–7.
10. Brautaset T, Sletta H, Nedal A, Borgos SEF, Degnes KF, Bakke I, et al. Improved antifungal polyene macrolides via engineering of the nystatin biosynthetic genes in *Streptomyces noursei*. Chem Biol. 2008;15(11):1198–206.
11. Carmody M, Murphy B, Byrne B, Power P, Rai D, Rawlings B, et al. Biosynthesis of amphotericin derivatives lacking exocyclic carboxyl groups. J Biol Chem. 2005;280(41):34420–6.
12. Seco EM, Fotso S, Laatsch H, Malpartida F. A tailoring activity is responsible for generating polyene amide derivatives in *Streptomyces diastaticus* var. 108. Chem Biol. 2005;12(10):1093–101.
13. Chen S, Mao X, Shen Y, Zhou Y, Li J, Wang L, et al. Tailoring the P450 monooxygenase gene for FR-008/candicidin biosynthesis. Appl Environ Microbiol. 2009;75(6):1778–81.
14. Qi Z, Kang Q, Jiang C, Han M, Bai L. Engineered biosynthesis of pimaricin derivatives with improved antifungal activity and reduced cytotoxicity. Appl Microbiol Biotechnol. 2015;99(16):6745–52.
15. Sheng Y, Ou Y, Hu X, Deng Z, Bai L, Kang Q. Generation of tetramycin B derivative with improved pharmacological property based on pathway engineering. Appl Microbiol Biotechnol. 2020;104(6):2561–73.
16. Byrne B, Carmody M, Gibson E, Rawlings B, Caffrey P. Biosynthesis of deoxyamphotericins and deoxyamphoteronolides by engineered strains of *Streptomyces nodosus*. Chem Biol. 2003;10(12):1215–24.
17. Chen S, Huang X, Zhou X, Bai L, He J, Jeong KJ, et al. Organizational and mutational analysis of a complete FR-008/candicidin gene cluster encoding a structurally related polyene complex. Chem Biol. 2003;10(11):1065–76.
18. Palacios DS, Anderson TM, Burke MD. A post-PKS oxidation of the amphotericin B skeleton predicted to be critical for channel formation is not required for potent antifungal activity. J Am Chem Soc. 2007;129(45):13804–5.
19. Mendes MV, Recio E, Fouces R, Luiten R, Martín JF, Aparicio JF. Engineered biosynthesis of novel polyenes: a pimaricin derivative produced by targeted gene disruption in *Streptomyces natalensis*. Chem Biol. 2001;8(7):635–44.
20. Volokhan O, Sletta H, Ellingsen TE, Zotchev SB. Characterization of the P450 monooxygenase NysL, responsible for C-10 hydroxylation during biosynthesis of the polyene macrolide antibiotic nystatin in *Streptomyces noursei*. Appl Environ Microbiol. 2006;72(4):2514–9.
21. Kim HJ, Kim MK, Lee MJ, Won HJ, Choi SS, Kim ES. Post-PKS tailoring steps of a disaccharide-containing polyene NPP in *Pseudonocardia autotrophica*. PLoS ONE. 2015;10(4): e0123270.
22. Lee MJ, Kong D, Han K, Sherman DH, Bai L, Deng Z, et al. Structural analysis and biosynthetic engineering of a solubility-improved and less-hemolytic nystatin-like polyene in *Pseudonocardia autotrophica*. Appl Microbiol Biotechnol. 2012;95(1):157–68.
23. Barke J, Seipke RF, Grüschow S, Heavens D, Drou N, Bibb MJ, et al. A mixed community of actinomycetes produce multiple antibiotics for the fungus farming ant *Acromyrmex octospinosus*. BMC Biol. 2010;8:109. https://doi.org/10.1186/1741-7007-8-109.
24. De Poire E, Stephens N, Rawlings B, Caffrey P. Engineered biosynthesis of disaccharide-modified polyene macrolides. Appl Environ Microbiol. 2013;79(19):6156–9.
25. Walmsley S, De Poire E, Rawlings B, Caffrey P. Engineered biosynthesis and characterisation of disaccharide-modified 8-deoxyamphoteronolides. Appl Microbiol Biotechnol. 2017;101(5):1899–905.
26. Caffrey P, Lynch S, Flood E, Finnan S, Oliynyk M. Amphotericin biosynthesis in *Streptomyces nodosus*: deductions from analysis of polyketide synthase and late genes. Chem Biol. 2001;8(7):713–23.
27. Cao B, Yao F, Zheng X, Cui D, Shao Y, Zhu C, et al. Genome mining of the biosynthetic gene cluster of the polyene macrolide antibiotic tetramycin and characterization of a P450 monooxygenase involved in the hydroxylation of the tetramycin B polyol segment. ChemBioChem. 2012;13(15):2234–42.
28. Aparicio JF, Fouces R, Mendes MV, Olivera N, Martín JF. A complex multienzyme system encoded by five polyketide synthase genes is involved in the biosynthesis of the 26-membered polyene macrolide pimaricin in *Streptomyces natalensis*. Chem Biol. 2000;7(11):895–905.
29. Santos-Aberturas J, Engel J, Dickerhoff J, Dörr M, Rudroff F, Weisz K, et al. Exploration of the substrate promiscuity of biosynthetic tailoring enzymes as a new source of structural diversity for polyene macrolide antifungals. ChemCatChem. 2015;7(3):490–500.
30. MacNeil DJ, Gewain KM, Ruby CL, Dezeny G, Gibbons PH, MacNeil T. Analysis of *Streptomyces avermitilis* genes required for avermectin biosynthesis utilizing a novel integration vector. Gene. 1992;111(1):61–8.
31. Bierman M, Logan R, O'Brien K, Seno ET, Rao RN, Schoner BE. Plasmid cloning vectors for the conjugal transfer of DNA from *Escherichia coli* to *Streptomyces* spp. Gene. 1992;116(1):43–9.
32. Gao HJ. Study on C-7′-N-methyltransferase gene *aprI* and regulatory gene *aprH* in apramycin biosynthesis pathway. Shenyang Pharmaceutical University. 2017.
33. Green MR, Sambrook J. Molecular cloning: a laboratory manual. 4th ed. Cold Spring Harbor: Cold Spring Harbor Laboratory Press; 2012.
34. Kieser T, Bibb MJ, Buttner MJ, Chater KF, Hopwood DA. Practical streptomyces genetics. Norwich: John Innes Foundation; 2000.
35. Bruheim P, Borgos SE, Tsan P, Sletta H, Ellingsen TE, Lancelin JM, et al. Chemical diversity of polyene macrolides produced by *Streptomyces noursei* ATCC 11455 and recombinant strain ERD44 with genetically altered polyketide synthase NysC. Antimicrob Agents Chemother. 2004;48(11):4120–9.
36. Seco EM, Cuesta T, Fotso S, Laatsch H, Malpartida F. Two polyene amides produced by genetically modified *Streptomyces diastaticus* var. 108. Chem Biol. 2005;12(5):535–43.
37. Won HJ, Kim HJ, Jang JY, Kang SH, Choi SS, Kim ES. Improved recovery and biological activities of an engineered polyene NPP analogue in *Pseudonocardia autotrophica*. J Ind Microbiol Biotechnol. 2017;44(9):1293–9.

Publisher's Note

Springer Nature remains neutral with regard to jurisdictional claims in published maps and institutional affiliations.